scientific reports

Check for updates

OPEN

Multimodal MRI analysis of COVID-19 effects on pediatric brain

Ting Peng[1,3,5], Chaowei Zhang[2,5], Pingping Xie[3,5], Ying Lin[1], Lin Zhang[4], Zuozhen Lan[4], Mingwen Yang[4], Xianghui Huang[1]✉, Jungang Liu[4]✉ & Guoqiang Cheng[1]✉

The COVID-19 pandemic has raised significant concerns regarding its impact on the central nervous system, including the brain. While the effects on adult populations are well documented, less is known about its implications for pediatric populations. This study investigates alterations in cortical metrics and structural covariance networks (SCNs) based on the Local Gyrification Index (LGI) in children with mild COVID-19, alongside changes in non-invasive MRI proxies related to glymphatic function. We enrolled 19 children with COVID-19 and 22 age-comparable healthy controls. High-resolution T1-weighted and diffusion-weighted MRI images were acquired. Cortical metrics, including thickness, surface area, volume, and LGI, were compared using vertex-wise general linear models. SCNs were analyzed for differences in global and nodal metrics, and MRI proxies, including diffusion tensor imaging along the perivascular space and choroid plexus (CP) volume, were also assessed. Our results showed increased cortical area, volume, and LGI in the left superior parietal cortex, as well as increased cortical thickness in the left lateral occipital cortex among children with COVID-19. SCN analysis revealed altered network topology and larger CP volumes in the COVID group, suggesting virus-induced neuroinflammation. These findings provide evidence of potential brain alterations in children following mild COVID-19, emphasizing the need for further investigation into long-term neurodevelopmental outcomes.

Keywords COVID, Structural covariance network, Glymphatic function

The COVID-19 pandemic has presented unprecedented challenges to both the physical and psychological well-being of individuals worldwide[1]. Now, in the fifth year of this global health crisis, mounting evidence indicates that SARS-CoV-2 exerts a detrimental impact on the central nervous system, particularly the brain. This viral influence has been linked to a range of neurological conditions, including headaches, dizziness, anosmia, ageusia, and cognitive impairments, all of which point to the virus's potential neurotropic properties[2–4]. Such findings underscore the virus's capacity to infiltrate the nervous system, posing significant challenges in understanding and managing its long-term neurological consequences[5].

Magnetic Resonance Imaging (MRI) has become a critical non-invasive technique for investigating the neuropathological mechanisms underlying brain alterations associated with COVID-19[6,7]. Several MRI studies have reported significant reductions in brain size, thinning of grey matter, disruptions in functional connectivity, and bilateral declines in glymphatic function in COVID-19 patients—changes that remain observable even months after recovery[7–12]. These structural and functional alterations may underlie the persistent neurological symptoms that many COVID-19 survivors continue to experience[13].

The early years of childhood are characterized by rapid, dynamic changes in brain structure, behavior, and cognition[14,15]. At the microstructural level, neurogenesis and synaptogenesis are occurring at a rapid pace, while the blood-brain barrier remains underdeveloped. At the macroscopic level, the brain undergoes significant morphological changes that further refine the separation and integration of brain functions[16–18]. Given that the first few years of life represent a critical window for brain development, it is plausible to hypothesize that COVID-19 infection could similarly affect brain structure and function in young children. While numerous studies have explored the impact of COVID-19 on the adult and elderly brain, research focusing on pediatric populations remains limited, primarily consisting of case reports and meta-analyses[19,20]. Consequently, there is a lack of quantitative data regarding the virus's impact on the developing brain in children.

[1]Fujian Key Laboratory of Neonatal Diseases, Children's Hospital of Fudan University (Xiamen Branch), Xiamen Children's Hospital, Xiamen 361000, China. [2]Department of Neonatology, People's Hospital of Longhua, Shenzhen 518000, China. [3]Department of Neonatology, Children's Hospital of Fudan University, Shanghai 201102, China. [4]Department of Radiology, Children's Hospital of Fudan University (Xiamen Branch), Xiamen Children's Hospital, Xiamen 361000, China. [5]Ting Peng, Chaowei Zhang and Pingping Xie contributed equally to this work. ✉email: xmhxh2013@163.com; jgliu_XMChospital@hotmail.com; gqcheng_cm@fudan.edu.cn

To address this critical gap, we recruited a cohort of children who had contracted mild COVID-19 and compared them with healthy controls (HCs). High-resolution structural and diffusion MRI data were collected to assess alterations in brain structure and function. Whole-brain vertex-wise morphometric analyses were performed, and structural covariance networks (SCNs) were constructed to evaluate the effects of COVID-19 on brain structure. SCNs are valuable for understanding how brain development, disease states, and shared environmental factors influence brain morphology[21,22]. Furthermore, diffusion tensor imaging along the perivascular space (DTI-ALPS), which assesses fluid flow along perivascular spaces crucial for waste clearance, and choroid plexus (CP) volume, which evaluates potential alterations in cerebrospinal fluid (CSF) production, were employed as MRI proxies to examine the function of the glymphatic system[23].

Methods

Participants

This study was conducted in accordance with the Declaration of Helsinki (revised in 2013) and received approval from the Ethics Committee of the Children's Hospital of Fudan University (Xiamen Branch), Xiamen Children's Hospital. Informed consent was obtained from the parents or guardians of all participants after a thorough explanation of the study's objectives. A total of 19 children (16 males, 3 females; mean age 3.4 ± 1.9 years) diagnosed with mild COVID-19 were enrolled based on the following inclusion criteria: (1) confirmed SARS-CoV-2 infection via antigen or polymerase chain reaction (PCR) testing; (2) at least two weeks post-recovery from infection, defined as both a negative SARS-CoV-2 test result and resolution of symptoms; (3) aged 1–6 years; (4) no history of primary or secondary neurological disease, such as craniocerebral injury, tumors, epilepsy, or meningitis; (5) no major or genetic conditions affecting growth, development, or cognition; and (6) no contraindications to MRI. The exclusion criteria were: (1) incomplete image acquisition; (2) poor image quality; and (3) inadequate image segmentation during preprocessing. The median interval between the onset of COVID-19 and MRI examination was 30.0 days (interquartile range [IQR]: 27.5, 34.5 days). Additionally, 22 age-comparable HCs (13 males, 9 females; mean age 3.9 ± 1.3 years) were recruited between February 2023 and May 2023. These controls had no history of SARS-CoV-2 infection (confirmed by antigen or PCR testing and self-reported history), no neurological disease, and no contraindications to MRI. All participants were of Han Chinese ethnicity, residing in Fujian, China.

According to the "Diagnosis, treatment and prevention of severe acute respiratory syndrome coronavirus 2 infection in children: experts' consensus statement (Fifth Edition)" published in China, the clinical classification of COVID-19 in children includes five categories: asymptomatic infection, mild, moderate, severe, and critical. Mild cases are mainly characterized by acute upper respiratory tract infection, which may be accompanied by fever, fatigue, headache, and muscle pain. General clinical data were obtained from the medical records system.

MRI acquisition

MRI scans were performed using a 3.0T MR scanner (uMR890, United Imaging, Shanghai, China) equipped with a 64-channel head coil at Xiamen Children's Hospital. To minimize head motion, foam padding was applied, and noise-canceling headphones were provided to reduce machine noise interference. High-resolution 3D T1-weighted structural MRI data were obtained using a GRE-FSP sequence with the following parameters: repetition time (TR) = 6.7 ms, echo time (TE) = 2.3 ms, flip angle = 8°, acquisition matrix = 320 × 300, field of view (FOV) = 256 × 240 mm, slice thickness = 0.8 mm, and spatial resolution = 0.8 × 0.8 × 0.8 mm. Diffusion-weighted images were acquired using an EPI-DTI sequence across three b-values (500, 1000, and 3000 s/mm^2) with 9, 12, and 48 non-collinear directions, respectively. The scan parameters were: TR = 3016 ms, TE = 77.1 ms, flip angle = 90°, acquisition matrix = 140 × 140, FOV = 210 × 210 mm, slice thickness = 1.5 mm, and spatial resolution = 1.5 × 1.5 × 1.5 mm.

Image processing

Structural images were processed using the FreeSurfer package (version 7.4.0; https://surfer.nmr.mgh.harvard.edu/) for cortical reconstruction and volumetric segmentation. The technical details of these procedures have been previously described in prior publications[24,25]. Cortical metrics, including cortical thickness, surface area, volume, and the Local Gyrification Index (LGI), were measured using surface-based morphometry principles. To enhance the robustness of the analysis, individual cortical metric maps were smoothed with a Gaussian kernel of 5 mm full-width at half maximum. The brain was parcellated into 68 cortical regions using the Desikan-Killiany (DK) atlas, and the mean LGI for each region was calculated[26]. Given the developmental characteristics of our pediatric sample (ages 1–6), additional steps were taken to ensure the accuracy of segmentation and parcellation results. Beyond the standard FreeSurfer pipeline, we also processed the data using Infant-FreeSurfer for validation purposes. All segmentation results were manually reviewed by two experienced pediatric neuroradiologists, who evaluated the anatomical plausibility of the parcellations. Our findings showed that for the 1-6-year-old cross-age sample, the standard FreeSurfer pipeline produced more stable and accurate results. Consequently, we based subsequent analyses on the segmentation results obtained from the standard FreeSurfer pipeline.

Diffusion images were preprocessed using MRtrix3 (version 3.0.4; https://www.mrtrix.org/) and DSI Studio (version 2022; https://dsi-studio.labsolver.org/) following the procedures outlined below[27]: (1) quality inspection; (2) conversion of NIFTI to the native MIF format; (3) denoising using random matrix theory[28]; (4) removal of Gibbs ringing artifacts[29]; (5) motion and distortion correction[30]; (6) bias field correction; (7) conversion of MIF back to NIFTI for further processing in DSI Studio; (8) creation of a mask to exclude background regions and enhance reconstruction accuracy; and (9) DTI-based reconstruction to characterize the major diffusion direction of the fibers.

Construction of structural covariance networks

SCNs based on the LGI were constructed using the Graph Analysis Toolbox (GAT)[31,32]. For each group, a 68 × 68 correlation matrix was established based on the DK atlas, with connection strength defined as Pearson correlation coefficients between LGI histograms of each pair of brain regions, adjusted for age, gender, and estimated Total Intracranial Volume (eTIV) (Fig. 1A, B). The SCNs were subsequently binarized using density thresholds ranging from 0.24 to 0.38 (with an increment of 0.01), ensuring that both HCs and COVID networks contained the same number of nodes and edges at each density (Fig. 1C, D). The minimum density (D_{min}) was set at 0.24 to maintain adequate connectivity and avoid network fragmentation in both groups. The density ranged from D_{min} to the maximum density at which the networks in both groups exhibited a small-world index (σ) greater than 1.2.

Global and nodal network metrics were calculated in accordance with established definitions from previous studies[33,34]. The global metrics included the clustering coefficient (Cp), characteristic path length (Lp), normalized clustering coefficient (γ), normalized characteristic path length (λ), σ, global efficiency (Eg), transitivity, and modularity. Nodal metrics included the nodal clustering coefficient, nodal degree, nodal betweenness centrality, and nodal local efficiency. Network hubs were identified as regions where the nodal betweenness centrality was at least 2 standard deviations larger than the average value[31]. The hubs of both groups were visualized using the BrainNet Viewer[35].

Calculation of DTI-ALPS index

Fractional anisotropy color maps were generated using DSI Studio. At the level of the lateral ventricle body, regions of interest (ROIs) with a 3 mm diameter were placed on bilateral projection and association fibers by an experienced neuroradiologist. Fiber orientation and diffusivities along the x-axis (right-left; Dxx), y-axis (antero-posterior; Dyy), and z-axis (infero-superior; Dzz) within the ROIs were obtained. The DTI-ALPS index for the left hemisphere (left ALPS) and right hemisphere (right ALPS) was calculated separately using the formula: DTI-ALPS index = mean (Dxxproj, Dxxassoc)/ mean (Dyyproj, Dzzassoc)[36]. A higher DTI-ALPS index indicates better glymphatic function.

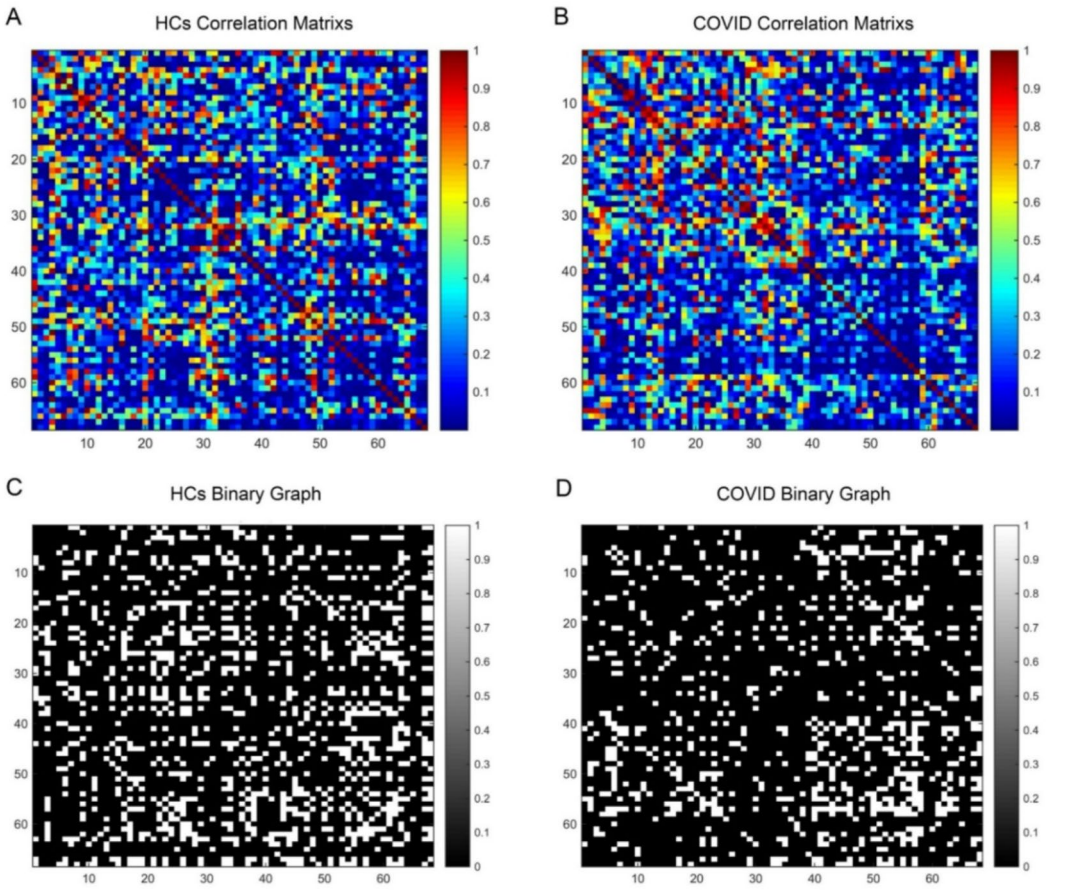

Fig. 1. Correlation and binary adjacency matrices for healthy controls (HCs) and COVID-19 patients. (**A**) Correlation matrix for HCs, (**B**) correlation matrix for COVID-19 patients, (**C**) binary adjacency matrix thresholded at D_{min} (0.24) for HCs, and (**D**) binary adjacency matrix thresholded at D_{min} (0.24) for COVID-19 patients. The color bar represents the correlation coefficient, indicating the strength of the connections between brain regions.

Estimation of CP volume

Bilateral CP volumes were obtained from the automatic segmentation of 3D T1-weighted images using FreeSurfer. To minimize interindividual variability, CP volume was normalized to the eTIV and multiplied by 1000, as recommended in prior studies[37]. A higher CP volume is indicative of increased CSF production.

Statistical analyses

Statistical analyses were conducted using IBM SPSS 23.0. Continuous variables are presented as mean ± standard deviation or median (IQR), while categorical variables are expressed as numbers (percentages). Group comparisons of continuous variables were performed using the independent samples t-test for normally distributed data, Welch's t-test for normally distributed data with unequal variances, or the Mann-Whitney U-test for non-normally distributed data. Categorical variables were compared using Chi-square tests. Statistical significance was determined using a two-tailed P-value of < 0.05.

Surface-based cortical metrics were compared between groups using vertex-wise general linear models in FreeSurfer, adjusted for age, gender, and eTIV. Multiple comparisons were controlled using vertex-wise $P < 0.01$ and cluster-wise $P < 0.05$. The area under the curve (AUC) for network parameters across all densities was calculated and compared between groups. A non-parametric permutation test with 1,000 repetitions was applied to assess significant differences in global and nodal network metrics. Comparisons of network metric were performed using the GAT toolbox, with statistical significance defined as $P < 0.05$, corrected for false discovery rate (FDR).

Results

Demographics

A total of 19 children diagnosed with COVID-19 and 22 HCs were included in the study. No significant differences were observed between the groups in terms of age (Z = -0.894, $P = 0.379$) or gender ($\chi^2 = 3.107$, $P = 0.098$). Additionally, there were no significant differences in eTIV between the groups (1,243,079.3 ± 166,049.0 mm^3 vs. 1,183,346.8 ± 161,198.2 mm^3; t = 1.164, $P = 0.251$). Among the COVID-19 patients, 14 (73.7%) experienced fever, 10 (52.6%) had a cough, 2 (10.5%) reported a headache, 2 (10.5%) had diarrhea, and 1 (5.3%) experienced myalgia.

Between-group comparisons of cortical metrics

Vertex-wise comparisons of cortical metrics are summarized in Table 1. Compared to the control group, the COVID-19 patients showed a significant increase in cortical area, volume, and LGI in the left superior parietal cortex. Additionally, cortical thickness was significantly increased in the left lateral occipital cortex (Monte Carlo correction, vertex-wise cluster threshold = 0.01, cluster-wise P-threshold = 0.05).

Between-group differences in global and nodal network parameters

To further investigate group differences, we assessed global and nodal network parameters based on cortical LGI. Changes in global network parameters across densities (ranging from 0.24 to 0.38) for the COVID and HCs groups are illustrated in Fig. 2. The COVID group exhibited a significantly lower Cp compared to the HCs, with significant difference observed at several density thresholds ($P < 0.05$, FDR-corrected; Fig. 2B). No significant differences were observed between the groups for the remaining parameters (Fig. 2). Notably, both groups' SCNs displayed small-world properties ($\sigma > 1.2$; Fig. 2I). The AUC comparisons further confirmed a significantly lower clustering coefficient in the COVID group ($P = 0.028$, FDR-corrected), while no other measures reached statistically significant between the groups.

AUC analyses of four nodal network measures—clustering coefficient, degree, betweenness centrality, and local efficiency—were also performed (Fig. 3). However, no significant differences between the groups were found after FDR correction.

Network hubs

Group-specific network hubs for the HCs and COVID groups are shown in Fig. 4. In the HCs, network hubs were identified in the left precuneus, left rostral middle frontal cortex, right pericalcarine cortex, right superior

Contrast COVID > HCs	Hemisphere	Cortical region	Size (mm^2)	Xyz peak (MNI)	*P*-value
Thickness	Left	Lateral occipital	201.90	-19.6/-96.1/-15.4	0.0171
Area	Left	Superior parietal	522.63	-21.9/-83.8/14.2	0.0004
Volume	Left	Superior parietal	224.45	-22.0/-66.5/30.6	0.0070
LGI	Left	Superior parietal	1548.83	-18.8/-70.8/38.3	0.0032

Age, gender, and eTIV were adjusted. Vertex-wise threshold $P<0.01$, cluster-wise threshold $P<0.05$.

Abbreviations: HCs, healthy controls; MNI, Montreal Neurological Institute; eTIV, total intracranial volume.

Table 1. Regional changes in cortical metrics in the children with COVID-19 compared with HCs.

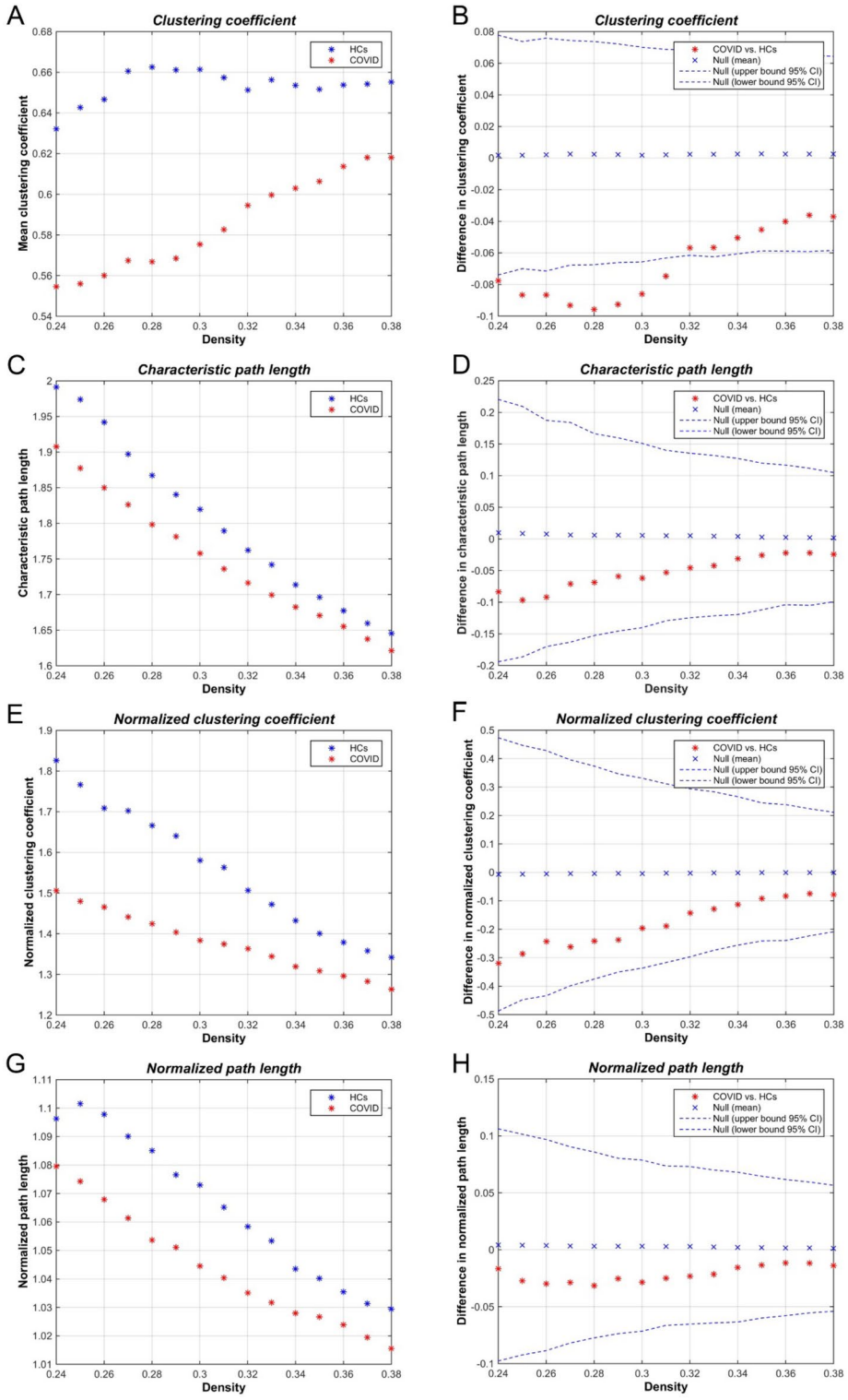

Fig. 2. Global network parameters for HCs and children with COVID-19, including between-group differences. (**A**,**B**) Clustering coefficient, (**C**,**D**) characteristic path length, (**E**,**F**) normalized clustering coefficient, (**G**,**H**) normalized path length, (**I**,**J**) small-world index, (**K**,**L**) global efficiency, (**M**,**N**) transitivity, and (**O**,**P**) modularity of the HCs and COVID-19 networks. Red * markers outside the 95% confidence interval (dashed lines) denote network densities with significant difference ($P < 0.05$). Positive values indicate higher densities in children with COVID-19 compared to HCs, while negative values indicate the opposite.

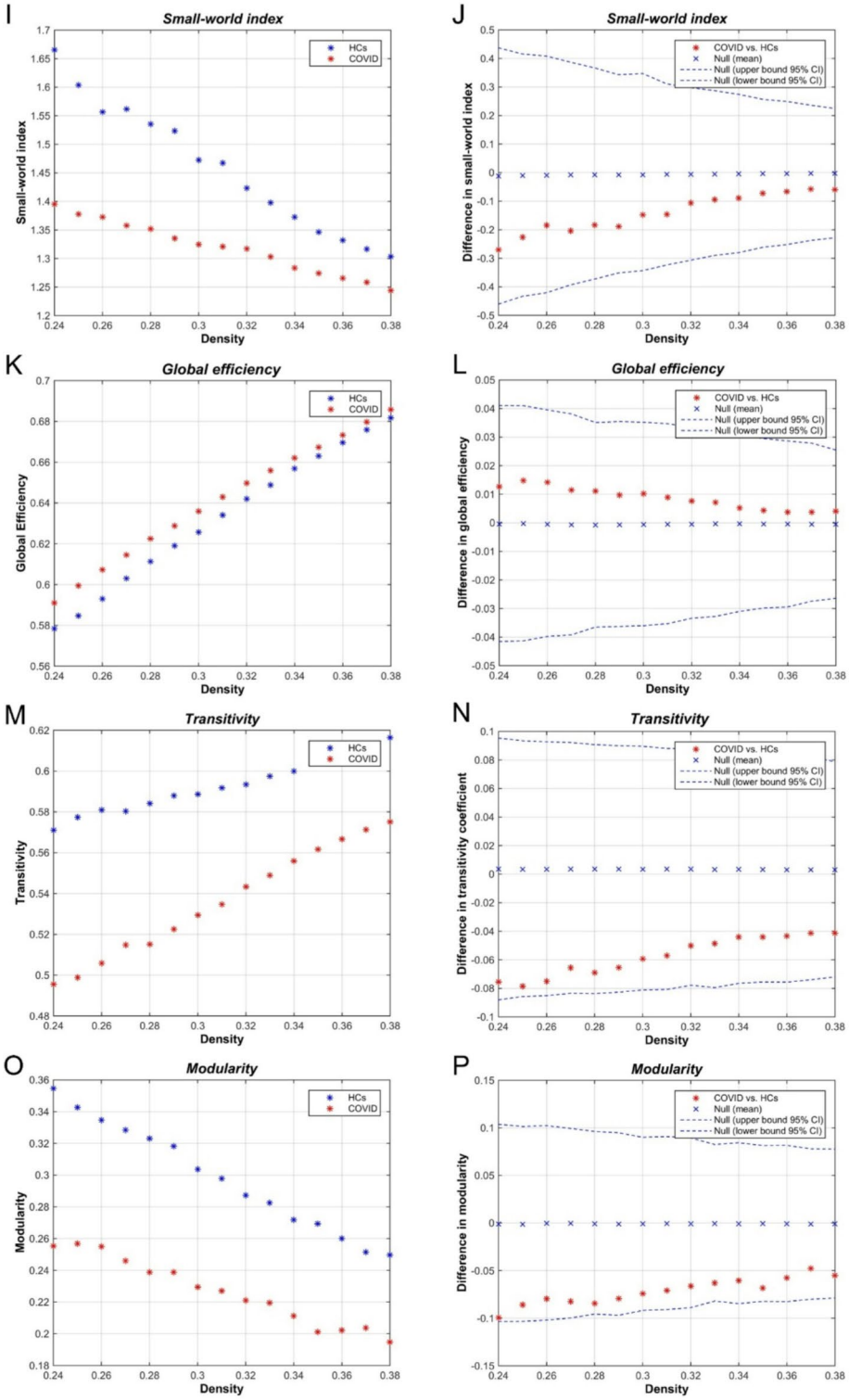

Figure 2. (continued)

parietal cortex, and right insula. In contrast, the number of hubs in the COVID group was reduced, with hubs identified only in the right postcentral and right precentral regions.

Between-group comparisons of DTI-ALPS index and CP volume

Figure 5; Table 2 illustrate the differences in bilateral DTI-ALPS index and CP volume between the COVID-19 patients and HCs. Compared to HCs, the COVID group showed significantly higher CP volumes in the left hemisphere (0.36 ± 0.13 vs. 0.28 ± 0.07, $P = 0.041$) and in total CP volume (0.40 ± 0.13 vs. 0.33 ± 0.07, $P = 0.043$).

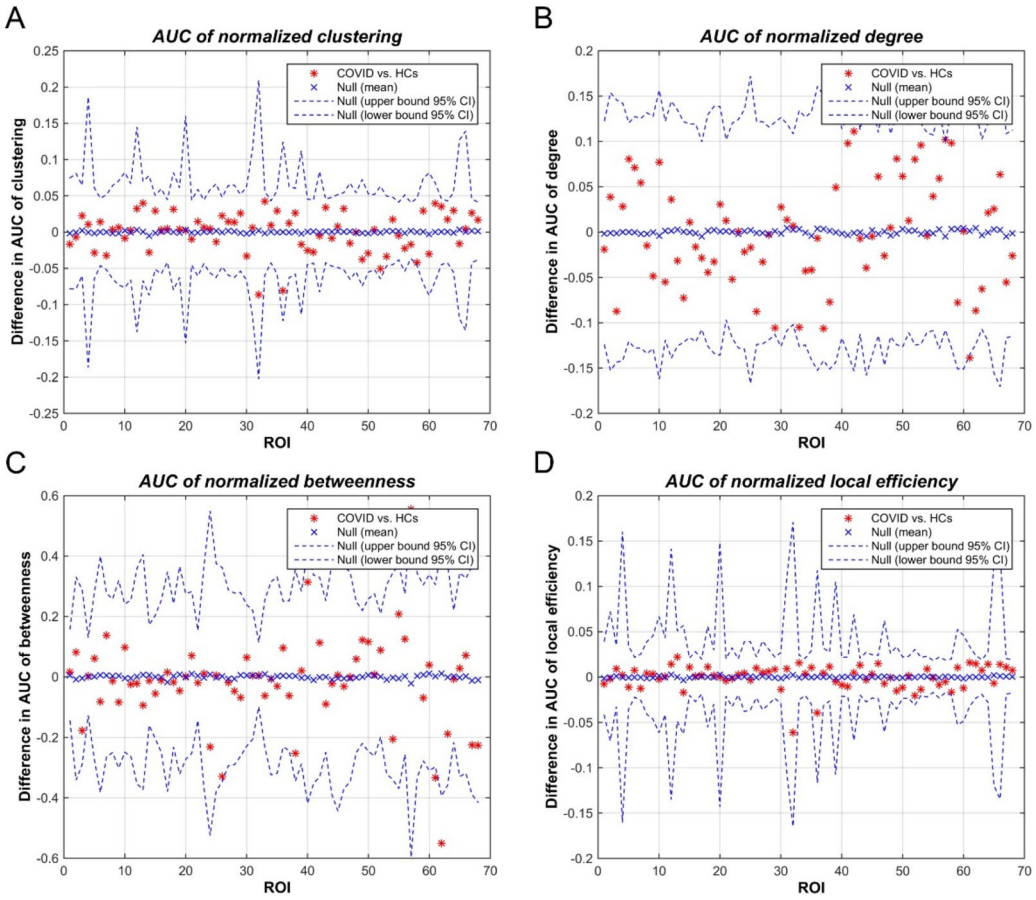

Fig. 3. Between-group differences in network parameters across a range of network densities: (**A**) normalized clustering coefficient, (**B**) normalized degree, (**C**) normalized betweenness, and (**D**) normalized local efficiency. Red * markers outside the 95% confidence interval indicate regions where the difference between the two groups at a given density is statistically significant.

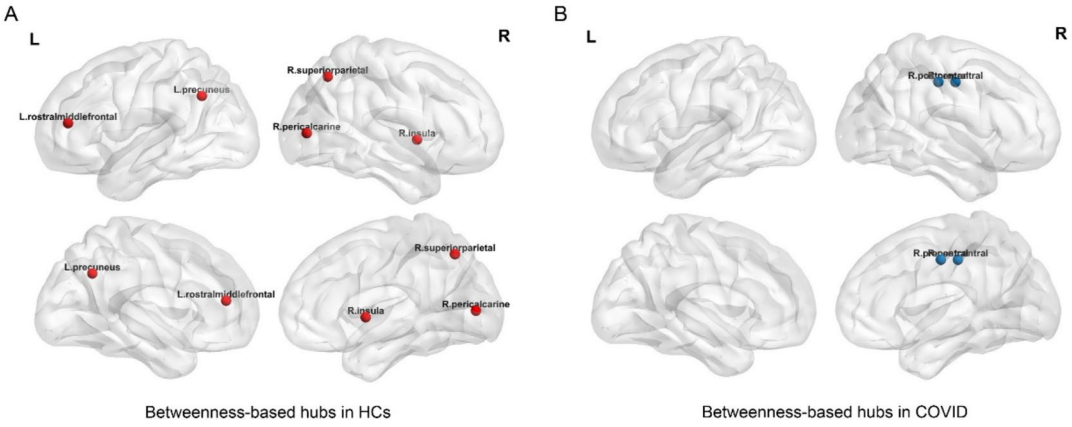

Fig. 4. Network hubs identified in the HCs (**A**) and COVID group (**B**). Five network hubs are highlighted in red for the HCs, while two network hubs are highlighted in blue for the COVID group.

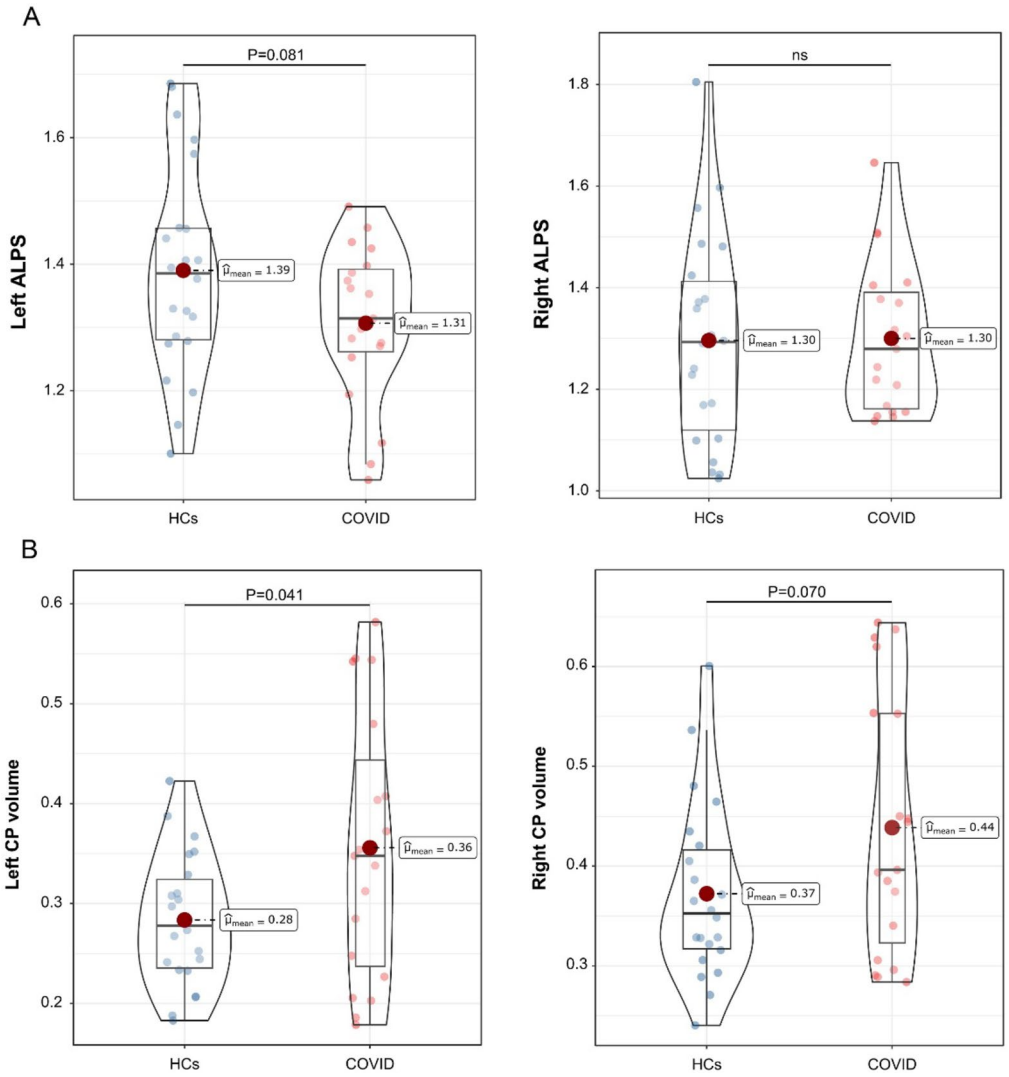

Fig. 5. Differences in DTI-ALPS index and choroid plexus (CP) volume between healthy controls (HCs) and children with COVID-19.

Variables	HCs (n=22)	COVID (n=19)	*P*-value
Total ALPS index	1.34±0.17	1.30±0.11	0.385
Left ALPS index	1.39±0.17	1.31±0.12	0.081
Right ALPS index	1.30±0.21	1.30±0.15	0.943
Total CP volume	0.33±0.07	0.40±0.13	0.043
Left CP volume	0.28±0.07	0.36±0.13	0.041
Right CP volume	0.37±0.09	0.44±0.13	0.070

Abbreviations: HCs, healthy controls; ALPS, along the perivascular space; CP, choroid plexus.

Table 2. ALPS index and choroid plexus (CP) volume.

However, no significant differences were observed between the groups in the left ALPS index (1.39 ± 0.17 vs. 1.31 ± 0.12, $P = 0.081$) or in right CP volume (0.37 ± 0.09 vs. 0.44 ± 0.13, $P = 0.070$).

Discussion

To the best of our knowledge, this study is the first to investigate the alterations in cortical morphometric parameters, LGI-based geometric networks, and glymphatic function in children with COVID-19. Our main findings include: (1) Children with COVID-19 exhibited significantly larger cortical area, volume, and LGI in the left superior parietal cortex, along with increased cortical thickness in the left lateral occipital cortex; (2) A reduction in the Cp of global network properties and alterations in network hubs were observed in young children with COVID-19, despite the absence of significant differences in regional network parameters; and (3) Both total and left CP volumes were higher in children with COVID-19 compared to HCs at least two weeks after recovery. These results suggest that abnormal cortical metrics, altered geometric networks, and potential glymphatic dysfunction may be consequences of COVID-19 in the developing brain.

The precise mechanisms through which COVID-19 induces neurological damage remain unclear. Current theories propose that SARS-CoV-2 may cause brain injury through direct invasion of the nervous system, disruption of the blood-brain barrier, vascular endothelial damage, and autoimmune responses[38]. The resulting dysregulated immune activation, neuroinflammation, and cytokine storms are believed to contribute to neurological dysfunctions in pediatric patients, with the severity of these effects correlating with the intensity of the disease[39–41]. These insights are consistent with our findings and provide a possible explanation for the observed alterations in cortical morphometric parameters and glymphatic function in children with COVID-19.

The observed increases in cortical area, volume, and LGI in the left superior parietal cortex may indicate heightened neuroplastic responses to COVID-19 in young children, potentially serving as compensatory mechanisms during critical developmental stages when this region plays a pivotal role in spatial cognition and sensorimotor integration[42]. Similarly, cortical thickening in the left lateral occipital cortex could reflect an adaptive neuroprotective response to preserve visual processing capabilities during the early stages of recovery[43]. These neurostructural patterns starkly contrast with established findings in adults, which demonstrate COVID-19-associated cortical thinning and gray matter reduction across multiple cohorts[7,10,11,13,44]. Systematic comparison with adult literature reveals partial overlap in the brain regions involved, despite the opposing morphological changes. Notably, studies have documented COVID-19-related cortical thinning in the left lateral occipital cortex among young adults with mild infections, while gray matter volume reductions in the left superior parietal cortex are correlated with cognitive deficits in adult patients[11,45]. However, no significant alterations in the cortical area of the left superior parietal cortex have been observed in adult patients[11,46]. Two key factors may explain these discrepancies. First, our study focused on a pediatric population aged 1–6 years, during a developmental stage when the brain may be more responsive or capable of compensating for the effects of COVID-19. Second, the cortical changes observed in our study represent an early or transient phase of the brain's response to infection, differing from the long-term effects reported in the adult literature. Longitudinal studies are necessary to determine whether these cortical changes represent protective adaptations, pathological markers, or precursors to later neurodevelopmental consequences. Such studies would provide a clearer understanding of the long-term impact of COVID-19 on pediatric brain development.

Notably, the abnormal brain regions identified in our study are predominantly localized to the left hemisphere. While the neurobiological mechanisms underlying this lateralization pattern require further investigation, our findings align with recent neuroimaging evidence on COVID-19. Specifically, Douaud et al. reported left-lateralized alterations in cortical thickness in adults with post-COVID conditions[7]. Similarly, Arrigoni et al. observed leftward-asymmetric microstructural abnormalities in structural connectivity among COVID-19 patients with persistent olfactory or cognitive deficits[47]. Furthermore, this lateralization pattern may not be limited to adults, as demonstrated by Invernizzi et al., who identified left-lateralized functional and structural brain alterations in adolescents following SARS-CoV-2 infection[13]. The consistency of these findings across diverse patient populations and imaging modalities suggests that SARS-CoV-2 infection may disproportionately affect left-hemispheric circuits involved in multisensory integration and higher-order cognitive processes.

In recent years, brain connectomics has emerged as a crucial tool for studying brain pathology[22,48]. To explore the neuroanatomical changes associated with mild COVID-19, we analyzed SCNs based on cortical LGI, revealing potential alterations in cortical connectivity linked to the disease. Our findings indicate that the COVID group exhibited a significantly lower Cp in global network properties compared to HCs, suggesting disruptions in local efficiency and possible segregation of cortical regions following COVID-19 (Fig. 2A, B). This may be attributed to neuroinflammation or other post-infectious processes[49]. Similar patterns have been observed in SCN studies of patients with ischemic moyamoya disease and individuals with autism spectrum disorder, highlighting the relevance of these findings[50,51]. Despite these disruptions, small-world properties were preserved in both groups, consistent with the brain's inherent resilience. Previous research on neurological conditions has noted that global efficiency often remains intact despite localized disruptions, suggesting the brain's capacity to maintain overall connectivity[52]. However, we did not observe significant differences in nodal network properties (Fig. 3), indicating that the effects of COVID-19 on brain connectivity may be subtle or dispersed across multiple nodes. This could contribute to the observed global network alterations without significantly affecting individual node characteristics. It is also possible that these nodal changes were too small to detect given the current sample size or statistical power. Additionally, the study identified network hubs in HCs distributed across the left precuneus, left rostral middle frontal cortex, right pericalcarine cortex, right superior parietal cortex, and right insula regions—areas typically involved in sensory integration and complex cognitive functions[53–56]. In contrast, the reduced hubs in the COVID group, concentrated in primary motor and sensory areas, suggest that COVID-19 may impair higher-order cognitive processing and multimodal integration[57,58].

The glymphatic system, which plays a crucial role in clearing brain waste through CSF circulation, is essential for maintaining the health of the nervous system[59,60]. A lower CP volume and a higher DTI-ALPS index have been associated with better glymphatic function[61–63]. In our study, we found significantly higher CP volumes in the left and total brain regions of COVID-19 patients compared to HCs, along with a trend towards a reduced left DTI-ALPS index in the patient group. The increased CP volume in the COVID group may indicate an underlying inflammatory response or altered CSF dynamics, potentially acting as a compensatory mechanism or as a consequence of viral invasion and immune activation[64,65]. Although the reduction in the left DTI-ALPS index was not statistically significant, it may suggest early-stage glymphatic dysfunction. Previous studies have reported significantly lower bilateral DTI-ALPS indices in COVID-19 patients four months post-infection compared to HCs[12]. The discrepancies in our findings could be attributed to several factors: first, our study may have captured an earlier stage of recovery; second, our cohort had fewer neurological symptoms and milder disease severity, which could influence glymphatic function; and third, limitations in sample size and imaging techniques may have affected the detection of statistically significant differences.

This study has several limitations. First, the small sample size and cross-sectional design may impact the robustness of our results and limit our ability to explore the long-term effects of COVID-19 on the developing brain. Future studies with larger sample sizes and longitudinal follow-up are needed to provide deeper insights. Second, the SCNs were constructed as group-level networks rather than individual networks for each participant. In future work, we plan to create individual-level networks, such as morphological similarity networks and morphometric inverse divergence networks, to provide a more detailed and personalized representation of network characteristics[66,67]. Third, using a more fine-grained atlas specifically designed for infants may offer more detailed information about the SCNs in children with COVID-19. Fourth, we did not collect clinical data from patients, which prevented us from analyzing correlations between clinical variables and cortical metrics, topological properties, and glymphatic system-related metrics. Lastly, as this is an exploratory study, we did not adjust for covariates such as age and gender in the group comparisons of glymphatic system-related metrics, which is another potential limitation.

In conclusion, our study provides the first report of changes in cortical metrics in young children with COVID-19, despite no observed differences in regional SCN parameters. We also employed a non-invasive multiparametric approach to assess the glymphatic function in COVID-19 patients. We speculate that viral-triggered neuroinflammation and immune response contribute to neurotoxic damage in brain regions involved in cognitive processing, ultimately resulting in alterations in cortical morphology and glymphatic function.

Data availability

All data generated or analyzed during this study are included in this published article. The raw data are available from the corresponding authors upon reasonable request.

Received: 12 September 2024; Accepted: 26 March 2025
Published online: 05 April 2025

References

1. Parotto, M. et al. Post-acute sequelae of COVID-19: Understanding and addressing the burden of multisystem manifestations. *Lancet Respiratory Med.* **11**, 739–754 (2023).
2. Shen, Q. et al. COVID-19: systemic pathology and its implications for therapy. *Int. J. Biol. Sci.* **18**, 386–408 (2022).
3. Chen, Y., Yang, W., Chen, F. & Cui, L. COVID-19 and cognitive impairment: neuroinvasive and blood–brain barrier dysfunction. *J. Neuroinflamm.* **19**, 222 (2022).
4. Hingorani, K. S., Bhadola, S. & Cervantes-Arslanian, A. M. COVID-19 and the brain. *Trends Cardiovasc. Med.* **32**, 323–330 (2022).
5. Losy, J. SARS-CoV-2 infection: symptoms of the nervous system and implications for therapy in neurological disorders. *Neurol. Therapy.* **10**, 31–42 (2021).
6. Meo, S. A., Abukhalaf, A. A., Alomar, A. A. & Al-Hussain, F. Magnetic resonance imaging (MRI) and neurological manifestations in SARS-CoV-2 patients. *Eur. Rev. Med. Pharmacol. Sci.* **25**, 1101–1108 (2021).
7. Douaud, G. et al. SARS-CoV-2 is associated with changes in brain structure in UK biobank. *Nature* **604**, 697–707 (2022).
8. Paolini, M. et al. Brain correlates of subjective cognitive complaints in COVID-19 survivors: A multimodal magnetic resonance imaging study. *Eur. Neuropsychopharmacol.* **68**, 1–10 (2023).
9. Wingrove, J. et al. Aberrant olfactory network functional connectivity in people with olfactory dysfunction following COVID-19 infection: an exploratory, observational study. *EClinicalMedicine* **58**, 101883 (2023).
10. Kamasak, B. et al. Effects of COVID-19 on brain and cerebellum: a voxel based morphometrical analysis. *Bratisl Med. J.*
11. Perlaki, G. et al. Gray matter changes following mild COVID-19: an MR morphometric study in healthy young people. *J. Magn. Reson. Imaging: JMRI*. https://doi.org/10.1002/jmri.28970 (2023).
12. Wu, L. et al. Glymphatic system dysfunction in recovered patients with mild COVID-19: A DTI-ALPS study. *iScience* 27, (2024).
13. Invernizzi, A. et al. Covid-19 related cognitive, structural and functional brain changes among Italian adolescents and young adults: a multimodal longitudinal case-control study. *MedRxiv: Preprint Serv. Health Sci.* **2023.07.19.23292909**. https://doi.org/10.1101/2023.07.19.23292909 (2023).
14. Li, G. et al. Computational neuroanatomy of baby brains: A review. *NeuroImage* **185**, 906 (2019).
15. Gilmore, J. H., Santelli, R. K. & Gao, W. Imaging structural and functional brain development in early childhood. *Nat. Rev. Neurosci.* **19**, 123–137 (2018).
16. Kostović, I. & Jovanov-Milosević, N. The development of cerebral connections during the first 20–45 weeks' gestation. *Semin Fetal Neonatal Med.* **11**, 415–422 (2006).
17. Innocenti, G. M. & Price, D. J. Exuberance in the development of cortical networks. *Nat. Rev. Neurosci.* **6**, 955–965 (2005).
18. Olin, A. et al. Stereotypic immune system development in newborn children. *Cell* **174**, 1277–1292e14 (2018).
19. Safadieh, G. H. & Majzoub, E. Abou Abbas, L. Neuroimaging findings in children with COVID-19 infection: a systematic review and meta-analysis. *Sci. Rep.* **14**, 4790 (2024).
20. Li, L., Liao, H., Kuang, X. & Jin, K. Clinical characteristics and outcomes of COVID-19-associated encephalopathy in children. *J. Neurovirol.* https://doi.org/10.1007/s13365-024-01202-1 (2024).
21. Geng, X. et al. Structural and maturational covariance in early childhood brain development. *Cereb. Cortex (New York N Y : 1991)* **27**, 1795–1807 (2017).

22. Yang, Y. et al. Gout is not just arthritis: abnormal cortical thickness and structural covariance networks in gout. *Front. Neurol.* **12**, 662497 (2021).
23. Naganawa, S. & Taoka, T. The glymphatic system: A review of the challenges in visualizing its structure and function with MR imaging. *Magn. Reson. Med. Sci.* **21**, 182–194 (2020).
24. Dale, A. M., Fischl, B. & Sereno, M. I. Cortical surface-based analysis. I. Segmentation and surface reconstruction. *NeuroImage* **9**, 179–194 (1999).
25. Fischl, B. et al. Automatically parcellating the human cerebral cortex. *Cereb. Cortex (New York N Y : 1991)*. **14**, 11–22 (2004).
26. Desikan, R. S. et al. An automated labeling system for subdividing the human cerebral cortex on MRI scans into gyral based regions of interest. *NeuroImage* **31**, 968–980 (2006).
27. Yeh, F. C. Shape analysis of the human association pathways. *NeuroImage* **223**, 117329 (2020).
28. Veraart, J. et al. Denoising of diffusion MRI using random matrix theory. *NeuroImage* **142**, 394–406 (2016).
29. Kellner, E., Dhital, B., Kiselev, V. G. & Reisert, M. Gibbs-ringing artifact removal based on local subvoxel-shifts. *Magn. Reson. Med.* **76**, 1574–1581 (2016).
30. Holland, D., Kuperman, J. M. & Dale, A. M. Efficient correction of inhomogeneous static magnetic field-induced distortion in Echo Planar Imaging. *NeuroImage* 50, 175–183 (2010).
31. Hosseini, S. M. H., Hoeft, F. & Kesler, S. R. GAT: A Graph-Theoretical analysis toolbox for analyzing Between-Group differences in Large-Scale structural and functional brain networks. *PLOS ONE* **7**, e40709 (2012).
32. Mak, E., Colloby, S. J., Thomas, A. & O'Brien, J. T. The segregated connectome of late-life depression: a combined cortical thickness and structural covariance analysis. *Neurobiol. Aging* **48**, 212–221 (2016).
33. He, Y., Chen, Z. & Evans, A. Structural insights into aberrant topological patterns of large-scale cortical networks in Alzheimer's disease. *J. Neuroscience: Official J. Soc. Neurosci.* **28**, 4756–4766 (2008).
34. Zhang, Y. et al. Abnormal topological organization of structural covariance networks in amyotrophic lateral sclerosis. *NeuroImage Clin.* **21**, 101619 (2019).
35. Xia, M., Wang, J. & He, Y. BrainNet viewer: a network visualization tool for human brain connectomics. *PloS One* **8**, e68910 (2013).
36. Taoka, T. et al. Evaluation of glymphatic system activity with the diffusion MR technique: diffusion tensor image analysis along the perivascular space (DTI-ALPS) in Alzheimer's disease cases. *Jpn J. Radiol.* **35**, 172–178 (2017).
37. Xie, Y. Enlarged choroid plexus in relapsing-remitting multiple sclerosis May lead to brain structural changes through the glymphatic impairment. *Multiple Scler. Relat. Disorders* (2024).
38. Harrison, A. G., Lin, T. & Wang, P. Mechanisms of SARS-CoV-2 transmission and pathogenesis. *Trends Immunol.* **41**, 1100–1115 (2020).
39. Kempuraj, D. et al. COVID-19, mast cells, cytokine storm, psychological stress, and neuroinflammation. *Neuroscientist: Rev. J. Bringing Neurobiol. Neurol. Psychiatry*. **26**, 402–414 (2020).
40. Stafstrom, C. E. Neurological effects of COVID-19 in infants and children. *Dev. Med. Child. Neurol.* **64**, 818–829 (2022).
41. L, da S. C. et al. Neuroinflammation and Brain Development: Possible Risk Factors in COVID-19-Infected Children. *Neuroimmunomodulation* 28, (2021).
42. Husain, M. & Nachev, P. Space and the parietal cortex. *Trends Cogn. Sci.* **11**, 30–36 (2007).
43. Colombari, E. et al. Beyond primary visual cortex: the leading role of lateral occipital complex in early conscious visual processing. *NeuroImage* **298**, 120805 (2024).
44. Díez-Cirarda, M. et al. Multimodal neuroimaging in post-COVID syndrome and correlation with cognition. *Brain* **awac384** https://doi.org/10.1093/brain/awac384 (2022).
45. Capelli, S. et al. MRI evidence of Gray matter loss in COVID-19 patients with cognitive and olfactory disorders. *Ann. Clin. Transl. Neurol.* **11**, 2457–2472 (2024).
46. Planchuelo-Gómez, Á. et al. Structural brain changes in patients with persistent headache after COVID-19 resolution. *J. Neurol.* **270**, 13–31 (2023).
47. Arrigoni, A. et al. Brain microstructure and connectivity in COVID-19 patients with olfactory or cognitive impairment. *Neuroimage Clin.* **43**, 103631 (2024).
48. Fornito, A., Zalesky, A. & Breakspear, M. The connectomics of brain disorders. *Nat. Rev. Neurosci.* **16**, 159–172 (2015).
49. Rubinov, M. & Sporns, O. Complex network measures of brain connectivity: uses and interpretations. *Neuroimage* **52**, 1059–1069 (2010).
50. Wang, P. et al. Reorganization of the brain structural covariance network in ischemic Moyamoya disease revealed by graph theoretical analysis. *Front. Aging Neurosci.* **14**, 788661 (2022).
51. Cai, S., Wang, X., Yang, F., Chen, D. & Huang, L. Differences in brain structural covariance network characteristics in children and adults with autism spectrum disorder. *Autism Res.* **14**, 265–275 (2021).
52. Wang, E. et al. Abnormal topological organization of sulcal Depth-Based structural covariance networks in Parkinson's disease. *Front. Aging Neurosci.* **12**, 575672 (2021).
53. Cavanna, A. E. & Trimble, M. R. The precuneus: a review of its functional anatomy and behavioural correlates. *Brain: J. Neurol.* **129**, 564–583 (2006).
54. Petrides, M. & Pandya, D. N. Dorsolateral prefrontal cortex: comparative cytoarchitectonic analysis in the human and the macaque brain and corticocortical connection patterns. *Eur. J. Neurosci.* **11**, 1011–1036 (1999).
55. Menon, V. & Uddin, L. Q. Saliency, switching, attention and control: a network model of Insula function. *Brain Struct. Funct.* **214**, 655–667 (2010).
56. Culham, J. C. & Kanwisher, N. G. Neuroimaging of cognitive functions in human parietal cortex. *Curr. Opin. Neurobiol.* **11**, 157–163 (2001).
57. Schulz, R. et al. Parietofrontal motor pathways and their association with motor function after stroke. *Brain: J. Neurol.* **138**, 1949–1960 (2015).
58. Alkadhi, H. et al. Reproducibility of primary motor cortex somatotopy under controlled conditions. *Am. J. Neuroradiol.* **23**, 1524–1532 (2002).
59. Mestre, H., Mori, Y. & Nedergaard, M. The brain's glymphatic system: current controversies. *Trends Neurosci.* **43**, 458–466 (2020).
60. Rasmussen, M. K., Mestre, H. & Nedergaard, M. The glymphatic pathway in neurological disorders. *Lancet Neurol.* **17**, 1016–1024 (2018).
61. Cai, X. et al. Diffusion along perivascular spaces provides evidence interlinking compromised glymphatic function with aging in Parkinson's disease. *CNS Neurosci. Ther.* **29**, 111–121 (2023).
62. Tian, Y. et al. Impaired glymphatic system as evidenced by low diffusivity along perivascular spaces is associated with cerebral small vessel disease: a population-based study. *Stroke Vasc Neurol.* **8**, e002191 (2023).
63. Tu, Y., Li, Z., Xiong, F. & Gao, F. Decreased DTI-ALPS and choroid plexus enlargement in fibromyalgia: a preliminary multimodal MRI study. *Neuroradiology* **65**, 1749–1755 (2023).
64. Ricigliano, V. A. G. & Stankoff, B. Choroid plexuses at the interface of peripheral immunity and tissue repair in multiple sclerosis. *Curr. Opin. Neurol.* **36**, 214–221 (2023).
65. Johnson, S. E. et al. Choroid plexus perfusion and intracranial cerebrospinal fluid changes after angiogenesis. *J. Cereb. Blood Flow. Metabolism: Official J. Int. Soc. Cereb. Blood Flow. Metabolism*. **40**, 1658–1671 (2020).
66. Seidlitz, J. et al. Morphometric similarity networks detect microscale cortical organization and predict Inter-Individual cognitive variation. *Neuron* **97**, 231 (2018).

67. Sebenius, I. et al. Robust Estimation of cortical similarity networks from brain MRI. *Nat. Neurosci.* **26**, 1461–1471 (2023).

Acknowledgements
This study was supported by the Key Program of the Xiamen Medical and Health (Grant No. 3502Z20234013).

Author contributions
TP, CZ, and PX contributed to data processing, analysis, and the writing of the original manuscript. YL, LZ, ZL, and MY were responsible for participant recruitment and data collection. XH, JL, and GC oversaw the study design and project coordination. All authors reviewed the manuscript.

Declarations

Competing interests
The authors declare no competing interests.

Ethical approval
The study was conducted in accordance with the Declaration of Helsinki (as revised in 2013) and was approved by the Ethics Committee of Xiamen Children's Hospital (No.2022-026). Informed consent was obtained from all participants and/or their legal guardians prior to their inclusion in the study.

Additional information
Correspondence and requests for materials should be addressed to X.H., J.L. or G.C.

Reprints and permissions information is available at www.nature.com/reprints.

Publisher's note Springer Nature remains neutral with regard to jurisdictional claims in published maps and institutional affiliations.

Open Access This article is licensed under a Creative Commons Attribution-NonCommercial-NoDerivatives 4.0 International License, which permits any non-commercial use, sharing, distribution and reproduction in any medium or format, as long as you give appropriate credit to the original author(s) and the source, provide a link to the Creative Commons licence, and indicate if you modified the licensed material. You do not have permission under this licence to share adapted material derived from this article or parts of it. The images or other third party material in this article are included in the article's Creative Commons licence, unless indicated otherwise in a credit line to the material. If material is not included in the article's Creative Commons licence and your intended use is not permitted by statutory regulation or exceeds the permitted use, you will need to obtain permission directly from the copyright holder. To view a copy of this licence, visit http://creativecommons.org/licenses/by-nc-nd/4.0/.

© The Author(s) 2025